

Pressure-induced Lifshitz transition in NbP: Raman, x-ray diffraction, electrical transport and density functional theory

Satyendra Nath Gupta¹, Anjali Singh^{2†}, Koushik Pal^{2†}, D.V.S.Muthu¹, C. Shekhar³, Yanpeng Qi³, Pavel G. Naumov³, Sergey A. Medvedev³, C. Felser³, U. V. Waghmare² and A. K. Sood^{1*}

*Department of Physics, Indian Institute of Science,
Bangalore-560012,India* ²*Theoretical Sciences Unit,*

Jawaharlal Nehru Centre for Advanced Scientific Research, Bangalore-560064,

India ³*Max Planck Institute for Chemical Physics of Solids,
01187 Dresden, Germany* [†]*These two authors contributed equally*

(Dated: September 28, 2017)

We report high pressure Raman, synchrotron x-ray diffraction and electrical transport studies on Weyl semimetals NbP and TaP along with first-principles density functional theoretical (DFT) analysis. The frequencies of first-order Raman modes of NbP harden with increasing pressure and exhibit a slope change at $P_c \sim 9$ GPa, and its resistivity exhibits a minimum at P_c . The pressure-dependent volume of NbP exhibits a change in its bulk modulus from 207 GPa to 243 GPa at P_c . Using DFT calculations, we show that these anomalies are associated with pressure induced Lifshitz transition which involves appearance of electron and hole pockets in its electronic structure. In contrast, results of Raman and synchrotron x-ray diffraction experiments on TaP and DFT calculations show that TaP is quite robust under pressure and does not undergo any phase transition.

PACS numbers:

I. INTRODUCTION

Soon after the discovery of Dirac equation in 1928, it was pointed out that another massless solution of the Dirac equation represents a new kind of particle called Weyl Fermions¹. The recent developments in topological insulators and topological semimetals have opened a way to realize Weyl Fermions in terms of low energy excitations where two non-degenerate linear dispersion electron bands cross each other at isolated points (called Weyl nodes) in Brillouin zone². This band structure has been observed in Weyl semimetals (WSMs)³⁻⁷. The Weyl nodes in WSMs always come in spatially separated pairs of opposite chirality, making WSMs different from Dirac semimetals which have two degenerate Weyl nodes that form one Dirac node due to time-reversal and inversion symmetry. WSMs exhibit many exotic properties induced by Weyl nodes like topological surface states with Fermi arcs^{3,4,6} and a negative longitudinal magnetoresistance due to the chiral anomaly⁸⁻¹⁵. Recently, the non-centrosymmetric TaAs, TaP, NbAs, and NbP have been predicted to be the candidate materials for WSMs with twelve pairs of Weyl nodes in their 3D Brillouin zones^{2,16}. The experimental evidence of Weyl nodes has been observed in this family by topological surface state and bulk electronic band structure measurements using angle resolved photoemission spectroscopy (ARPES)^{3,17,18}.

The Fermi surface topology of Weyl semimetals can be modified by a small change in the Fermi energy, due to their low intrinsic charge carrier densities. Application of pressure is known to be a powerful approach to tune the electronic and lattice structure of the material. High pressure synchrotron x-ray study of TaAs up to 53 GPa along with ab initio calculations¹⁹ show that TaAs goes

to hexagonal $P\bar{6}m2$ phase at 14 GPa from the ambient $I4_1md$ phase, along with changes in the electronic states. Further high pressure magneto-transport study up to 2.3 GPa of NbAs²⁰ shows that the Fermi surface exhibits an anisotropic evolution under pressure. Similarly magneto-transport study of NbP up to 2.8 GPa²¹ shows significant effect on the amplitudes of Shubnikov-de Haas oscillations due to the subtle changes in the Fermi surface. The effect of pressure on lattice and phonons has not been studied in NbP as well as in TaP. The objective of the present study is to examine NbP and TaP under pressure (carried out upto 25 GPa) using Raman spectroscopy and synchrotron x-ray diffraction as well as electrical transport (for NbP). DFT calculations have been done to gain microscopic insight into pressure effect. Our main results for NbP are: (i) The phonon frequencies of first order Raman modes exhibit slope change at $P_c \sim 9$ GPa, (ii) The resistivity of NbP pass through a minimum at P_c , (iii) The bulk modulus shows an increase at P_c , (iv) The DFT calculations reveal that these anomalies at P_c are due to Lifshitz transition involving appearance of electron and hole pockets in its electronic structure. In comparison to NbP, our results on TaP show no phase transition up to 27 GPa.

II. EXPERIMENTAL DETAILS

High-quality single crystals of NbP and TaP were grown via a chemical vapor transport reaction using iodine as a transport agent²². Initially, polycrystalline powder of NbP was synthesized by a direct reaction of niobium (Chempur 99.9%) and red phosphorus (Heraeus 99.999%) kept in an evacuated fused silica tube

for 48 hours at 800 °C. Starting from this microcrystalline powder, the single-crystals of NbP were synthesized by chemical vapor transport in a temperature gradient starting from 850 °C (source) to 950 °C (sink) and a transport agent with a concentration of 13,5 mg/cm³ iodine (Alfa Aesar 99,998%). Similar route was used for the growth of TaP crystals. Raman experiments were carried out at room temperature on these well characterized single crystals of NbP and TaP^{10,23} using confocal Horiba 800 spectrometer, peltier cooled CCD and 532 nm diode laser. The high pressure synchrotron x-ray diffraction measurements were done at DESY on the beam line (P02) using 0.2888Å x-ray radiation. Pressure was generated using a diamond anvil cell (DAC), where a thin platelet ($\sim 100\mu\text{m}$) of single crystals of NbP/TaP, was embedded in a 4:1 methanol: ethanol pressure transmitting medium along with a ruby chip for pressure calibration into a stainless steel gasket inserted between the diamonds. The electrical resistivity at different pressures was measured by the direct current van der Pauw technique in an in-house-designed diamond-anvil cell equipped with diamond anvils with a 500 μm culet. A cleaved NbP single crystal of a suitable size was cut and placed into the central hole of a tungsten gasket with an insulating cubic BN/epoxy layer without pressure transmitting medium. The electrical leads fabricated from 5 μm thick Pt foil were attached to the sample. The pressure was again determined by the ruby luminescence method.

III. COMPUTATIONAL DETAILS

Our first-principles calculations are based on density functional theory (DFT) as implemented in Quantum ESPRESSO package²⁴, in which the interaction between ionic cores and valence electrons is modeled with ultrasoft pseudopotentials²⁵. The exchange-correlation energy of electrons is treated within a Local Density Approximation (LDA) using a functional form parameterized by Perdew-Zunger²⁶. We use an energy cutoff of 60 Ry to truncate the plane wave basis for representing Kohn-Sham wave functions, and energy cutoff of 600 Ry on the basis set to represent charge density. We relaxed structures to minimize energy till the magnitude of Hellman-Feynman force on each atom is less than 0.03 eV/Å. In self-consistent Kohn-Sham (KS) calculations with primitive cells, the Brillouin zone (BZ) integrations were sampled with a uniform mesh of 11x11x11 k-points. We determined electronic structure by including the spin-orbit coupling (SOC) through use of relativistic ultrasoft pseudopotentials²⁷. We determined dynamical matrices and phonons at wavevectors on a 2x2x2 mesh in the BZ using DFT linear response (Quantum ESPRESSO implementation based on Green's function). We used scalar relativistic pseudopotential for phonon calculations as inclusion of SOC changed phonon frequencies by a very small value ($< 1 \text{ cm}^{-1}$) (Fig. 9c, d). To determine the

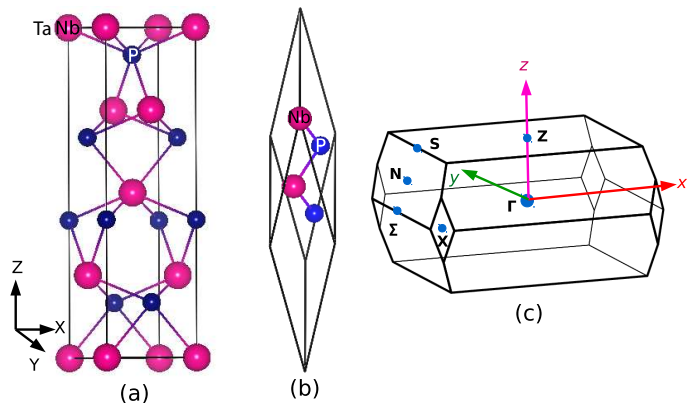


FIG. 1: (Color online) Crystal structure of bulk NbP and TaP with (a) conventional, (b) primitive unit cells and (c) their Brillouin zone (BZ).

bulk modulus (B), we have fitted the P vs V plot to Birch Murnaghan equation of state.

$$P(V) = \frac{3B}{2} \left[\left(\frac{V_0}{V} \right)^{\frac{7}{3}} - \left(\frac{V_0}{V} \right)^{\frac{5}{3}} \right] \left[1 + \frac{3}{4} (B' - 4) \left(\left(\frac{V_0}{V} \right)^{\frac{2}{3}} - 1 \right) \right] \quad (1)$$

where V is the volume at pressure P, V_0 is the reference volume, B is the bulk modulus, and B' is the pressure derivative of the bulk modulus. Fermi surfaces are interpolated on dense k-grids (equivalent to 33x33x33 in the whole BZ).

IV. RESULTS AND DISCUSSIONS

A. Experimental Results

NbP and TaP have the same geometric structure (non-centrosymmetric body centered tetragonal (BCT) structure), which belongs to the space group of $I4_1md$ (C_{4v}^{11} , no. 109)²⁸ with two atoms each of transition metal and phosphorous per primitive cell (see Fig. 1a, b). In this structure, Nb/Ta and P atoms have six nearest neighbors in a trigonal prismatic coordination. To understand the crystal structure, we can consider a stack of square lattice planes, where each plane is formed of either Nb/Ta or P atoms. Each plane is shifted by half a lattice constant in either direction (x or y) relative to the one below it. Due to these shifts, a screw pattern arises in the lattice along the z-direction leading to a non-symmorphic C_4 rotational symmetry that requires a translation along the z direction by $c/4$. It is clear from this crystal structure that NbP and TaP lack the spatial inversion symmetry. If time-reversal symmetry is respected, the broken inversion symmetry is an important condition for the Weyl semimetallic phase.

According to factor group analysis, this system has $[A_1+E]$ acoustic phonons and $[A_1+2B_1+3E]$ optical

phonons. All the optical phonons are Raman active²⁹. Fig.2 (a) shows Raman spectra of NbP at a few typical pressures. Five Raman modes are observed in NbP and assigned to E^1 , B_1^1 , E^2 , A_1 and B_1^2 irreducible representations, based on first-principles calculations (discussed latter). The Lorentzian line shapes were fitted to the Raman spectra to extract the phonon frequencies and full width at half maximum (FWHM). The Raman modes E^1 , B_1^1 and E^2 become very weak after ~ 9 GPa, making it difficult to follow them. The extracted phonon frequencies at different pressures, plotted in Fig.3 (a), show clearly that the phonon frequencies of A_1 and B_1^2 modes

exhibit a change in the slope $S \left(\frac{d\omega}{dP} \right)$ at $P_c \sim 9$ GPa, signifying a phase transition. To further investigate this transition, we did resistivity measurements as function of pressure. Fig.4 shows that the resistivity first decreases with increasing pressure and then increases, showing a minimum at P_c . Thus our Raman and resistivity results as a function of pressure show a phase transition at P_c . To find out structural changes, if any, at P_c , high pressure x-ray diffraction measurements were carried out. Fig.5 (a) shows x-ray diffraction patterns at a few representative pressures, revealing no new diffraction peaks or vanishing of the existing peaks till 25 GPa. This rules out the possibility of structural change at P_c . In order to get the lattice parameters, we did Rietveld refinement using Jana 2006³⁰ as shown for example at 0.6 GPa in Fig.5 (b). The diffraction pattern is well fitted by Jana 2006 at all pressures. Fig.5 (c) shows pressure dependence of the unit cell volume per formula unit (z). The solid red lines are fit to Eq.(1). It is clear from Fig.5 (c) that P-V data fitted using Eq. (1) (keeping B' fixed at 5) shows a clear change in bulk modulus: $B=207$ GPa ($P \leq P_c$) and 243 GPa ($P \geq P_c$). Thus high pressure x-ray data rules out a structural phase transition at P_c and suggests an isostructural electronic phase transition^{31–33}.

We will now present our results on TaP. Fig.2 (b) shows Raman spectra of TaP at a few representative pressures. As before, the solid red lines are the Lorentzian function fitted to the experimental data (black lines). At low pressure, only 3 modes could be recorded and the two other modes (E^1 and E^2) could be seen at higher pressures. The zero pressure extrapolated values of the frequencies of E^1 and E^2 modes are close to the values obtained from DFT calculations. The pressure dependence of phonon frequencies of E^1 , B_1^1 , E^2 , A_1 and B_1^2 modes are shown in Fig.6 (a). It is clear from Fig.6 (a) that all the Raman modes harden with increasing pressure and there is no slope change with pressure which is in contrast to the results obtained in NbP. Fig.7 (a) shows the pressure dependence of synchrotron x-ray diffraction patterns of TaP at a few pressures. We note that the number of diffraction peaks remain the same in the entire pressure range, suggesting no structural phase transition. The lattice parameters were obtained by Rietveld refinement using Jana 2006³⁰. The pressure dependence of the volume per formula unit (z) is shown in Fig.7 (b). The solid

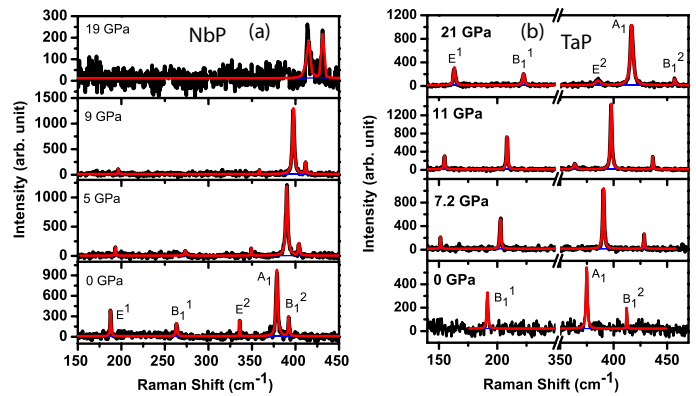


FIG. 2: (Color online) Raman spectrum of NbP (a) and TaP (b) at a few representative pressures. The solid lines (red and blue) are the Lorentzian fit to the measured spectra (black).

red line is the fit to Birch Murnaghan equation of state (Eq.1), showing that there is no change in the bulk modulus of TaP over the entire pressure range (Fig.7 (b)). We can thus conclude that TaP does not show any phase transition till 27 GPa.

B. Theoretical calculations

The calculated structural parameters are as follows: For NbP: $a=b=3.31\text{\AA}$, $c=11.23\text{\AA}$; for TaP: $a=b=3.29\text{\AA}$, $c=11.2\text{\AA}$. These values are in good agreement with experiments³⁴. Lattice structural parameters of bulk NbP and TaP show smooth variation as a function of hydrostatic pressure (Fig. 8 a,b), signifying the robustness of the crystal structure of NbP and TaP upto 20 GPa. Further, the absence of anomalies in c/a ratio rules out the possibility of an isostructural phase transition. Calculated bulk moduli (from V vs P plot Fig. 8 a,b) of the BCT structure of NbP (TaP) are 205 ± 0.4 GPa (215 ± 0.8 GPa), which agree well with experimental values of 207 ± 9 GPa (225 ± 5 GPa). Also, there is a change in the bulk modulus of NbP at 12 GPa, consistent with the experiment.

The electronic structure and phonon dispersion of NbP and TaP with and without spin-orbit coupling at 0 GPa are shown in Fig.9. In the absence of spin-orbit coupling, the valance band maximum (VBM) and conduction band minimum (CBM) cross the Fermi level along high symmetric paths (Γ - Σ -S-Z-N) of the Brillouin zone (Fig. 9a, b). This crossing leads to formation of closed ring structure (nodal rings²) (in $k_x = 0$ and $k_y = 0$ planes) which is based on the fact that bands have opposite eigenvalues of mirror symmetry. As spin-orbit coupling is introduced, the nodal rings disappear, *i.e.* gap opens up along these high-symmetry lines (refer blue line in Fig. 9a, b) and Weyl nodes are generated³⁴. This gap is smaller in NbP as compared to TaP, as expected from a weaker spin-orbit coupling in Nb as compared to Ta compounds. Our calculated phonon frequencies at zone center are in good

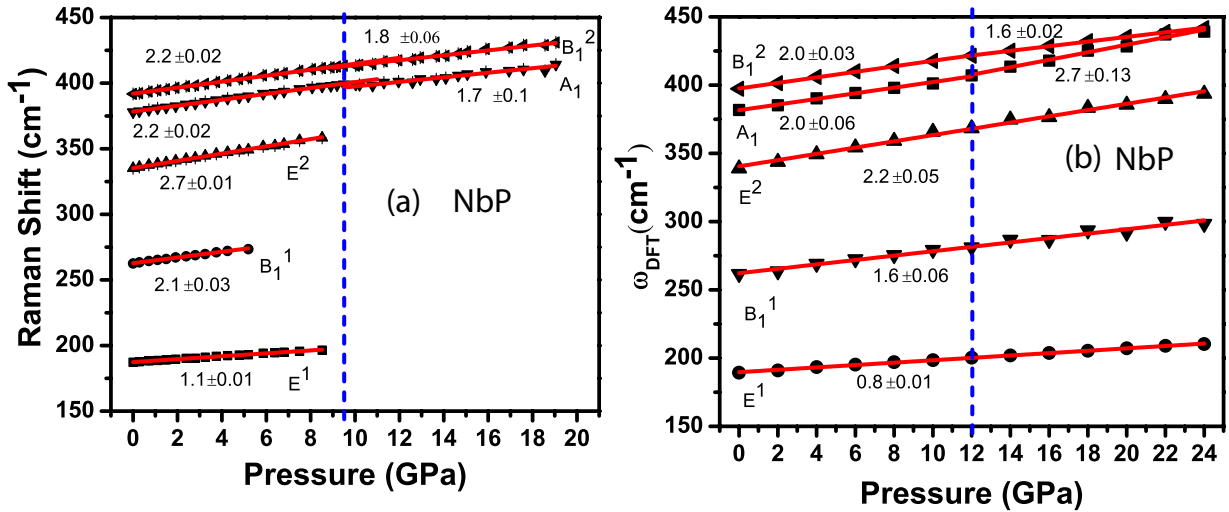


FIG. 3: (Color online) Pressure dependence of phonons of NbP: (a) Experiment; (b) Theory. The solid lines are the linear fit to the data. The slope S in the unit of $\text{cm}^{-1}/\text{GPa}$ is given near each of the the lines. The vertical dashed lines mark the transition pressure P_c

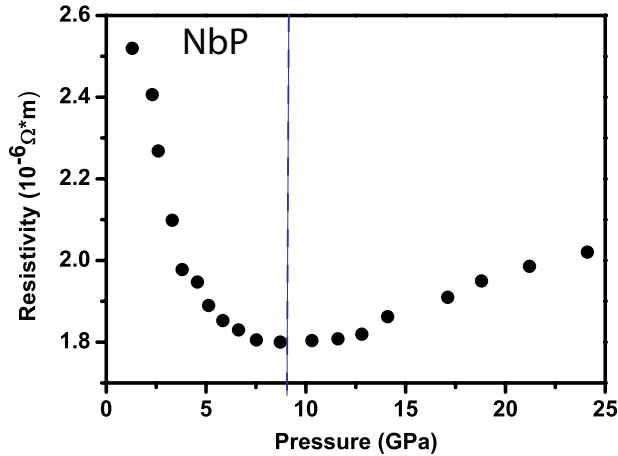


FIG. 4: (Color online) Measured resistivity of NbP as a function of pressure. The resistivity passes through a minimum at ~ 9 GPa as indicated by a vertical dashed line.

agreement with experiments (see Table I).

Our calculations of phonon frequencies of NbP as a function of hydrostatic pressure (Fig. 3 (b)) reveal that A_1 and B_1^2 modes exhibit change in S at $P_c^{theory} \sim 12$ GPa while the other three modes E^1 , E^2 and B_1^1 do not show any slope change till 24 GPa, consistent with the experimental results. The difference between the observed transition pressure $P_c \sim 9$ GPa and the calculated one $P_c^{theory} \sim 12$ GPa is partly due to the errors in calculated equilibrium lattice constants. To identify if it is a the structural phase transition, we considered two high symmetry crystal structures: (a) hexagonal (Tungsten Carbide structure with space group P-6m2, No. 162) and (b) cubic (CsCl structure with space group Pm-3m, No. 221), and calculated the enthalpy differences be-

TABLE I: Comparison of the observed and calculated frequencies of Raman active modes of NbP and TaP at 0 GPa. Excellent agreement between theory and experiment is evident.

Modes	NbP (0 GPa, ω in cm^{-1})		TaP (0 GPa, ω in cm^{-1})	
	Experiment	Theory	Experiment	Theory
E^1	189	182	145	146
B_1^1	263	262	191	192
E^2	335	339	341	339
B_1^2	391	397	411	415
A_1	377	382	373	375

tween these phases and the low pressure BCT structure. Although enthalpy difference (ΔH) between the hexagonal and BCT phase first increases slightly with pressure and then decreases, it does not attain negative value (Fig. 10a). Thus, a structural phase transition from BCT to hexagonal phase is ruled out. Similarly, ΔH , between the cubic and BCT phase decreases with pressure but does not crossover to negative value up to 24 GPa (inset of Fig. 10a), ruling out a structural phase transition to cubic phase as well. Our conclusion of the absence of a structural phase transition in NbP with pressure is consistent with our x-ray diffraction experiments.

To understand the origin of change in pressure coefficients of Raman active modes (A_1 and B_1^2 modes) of NbP above $P_c^{theory}=12$ GPa, we study the evolution of electronic structure with pressure. At $P = 0$ GPa, NbP is semimetallic in nature *i.e.* finite density of states at Fermi level. Near the Fermi energy, electronic structure of NbP at 0 GPa shows presence of electron pocket along Γ - Σ and hole pockets along S-Z and Z-N lines (refer Fig. 11a). As the hydrostatic pressure does not alter

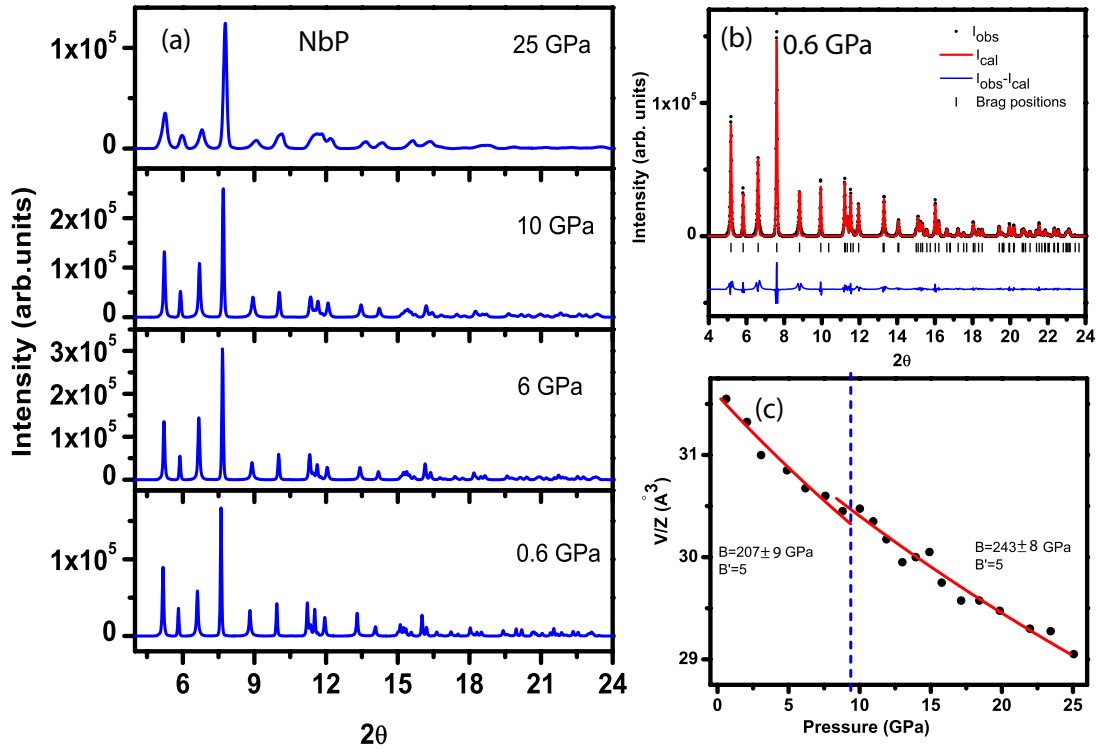


FIG. 5: (Color online) (a) X-ray diffraction pattern of NbP as a function of pressure. (b) The Rietveld refinement of X-ray diffraction pattern at 0.6 GPa pressure. (c) Pressure dependence of volume per formula unit (z) of NbP. The vertical dashed line indicates the transition pressure, at which bulk modulus changes.

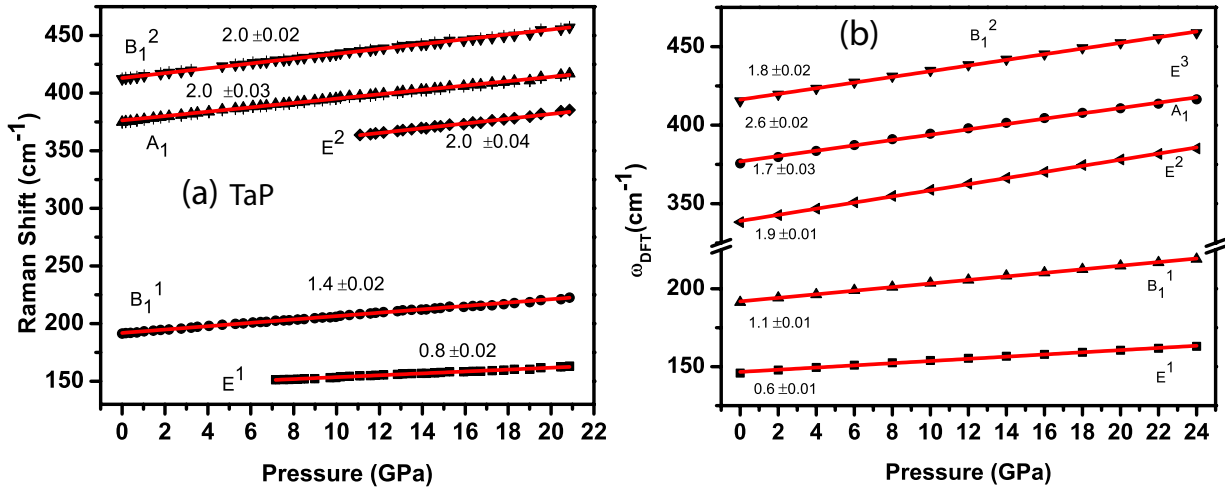


FIG. 6: (Color online) Pressure dependence of phonons of TaP: (a) Experiments; (b) Theory. The solid lines are the linear fit to the experimental data. The slope S in the unit of $\text{cm}^{-1}/\text{GPa}$ is given near the lines.

the symmetry of the crystal, energy levels do not split, but those near the Fermi energy change notably giving rise to pressure induced transfer of electrons from one pocket to another in order to maintain the total number of carriers (*i.e.* size of electron and hole pockets changes with pressure)³⁵. Interestingly, at 12 GPa a small hole pocket appears along Γ -N path (see Fig. 11c). To probe this further, we monitored the evolution of Fermi surface

with pressure, particularly the electron (red surface) and hole (blue surface) pockets (Fig. 12a). Electron and hole pockets are almost semicircular and distributed along the rings^{2,16} on the $k_x = 0$ and $k_y = 0$ mirror planes in the BZ (Fig. 12b). At 8 GPa, the size of electron pocket in vicinity of N-point reduces and a set of electron-pockets (in between existing hole pocket and one appearing near N-point) and hole-pockets (in vicinity of N-point) ap-

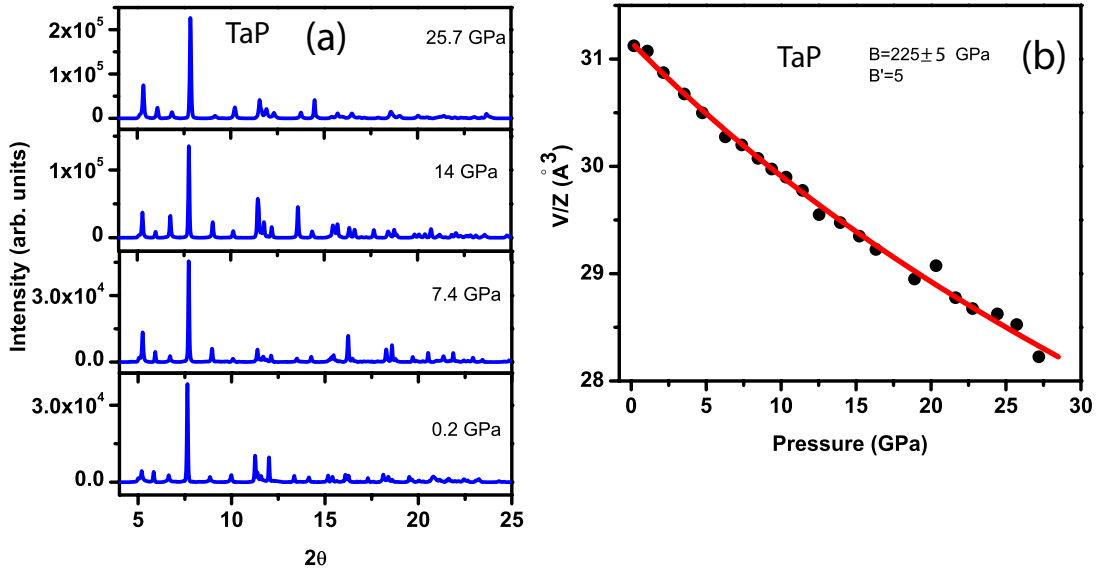


FIG. 7: (Color online) (a) X-ray diffraction pattern of TaP as function of pressure, and (b) pressure dependence of volume per formula unit (z) of TaP.

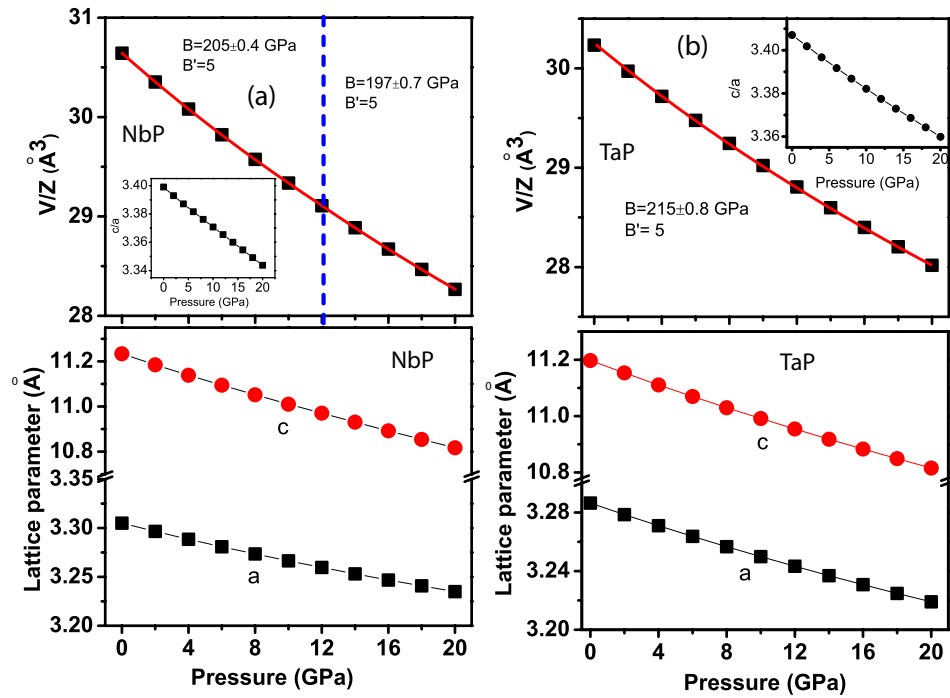


FIG. 8: (Color online) Calculated lattice structural parameters a , c , c/a and volume per formula unit of bulk NbP (a) and TaP (b) as a function of pressure.

pear (see Fig. 12c). Further increase in pressure results in changes of the shape and size of electron and hole pockets (refer Fig. 12). Note that the electron pocket in vicinity of Σ -point (Fig. 12a) does not disappear completely with increasing pressure. It is thus clear that there is notable changes in topology of Fermi surface with pressure.

Since, the Fermi surface changes with applied pressure without breaking the structural symmetry, we assign it as a Lifshitz transition occurring at P_c^{theory} . We note that there are changes in S at 12 GPa (Fig. 3b). Thus, there is a clear correlation between the pressure coefficients of Raman active modes and electronic phase tran-

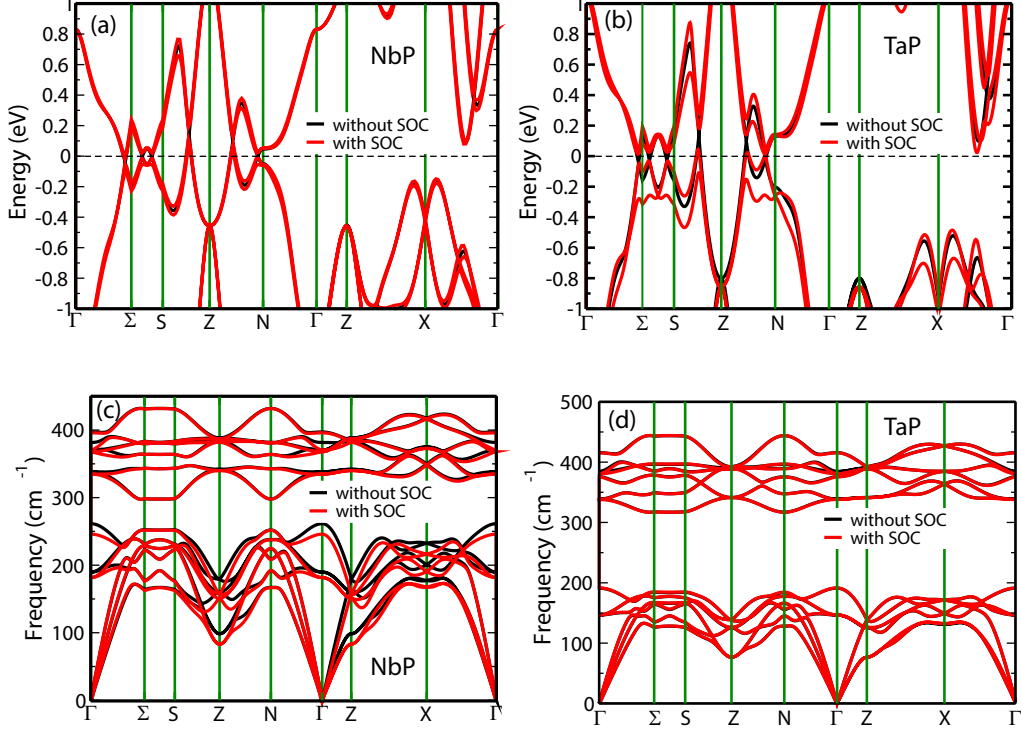


FIG. 9: (Color online) Electronic structure (a, b) and phonon dispersion (c, d) of bulk NbP and TaP respectively at $P = 0$ GPa, calculated with and without inclusion of spin-orbit coupling.

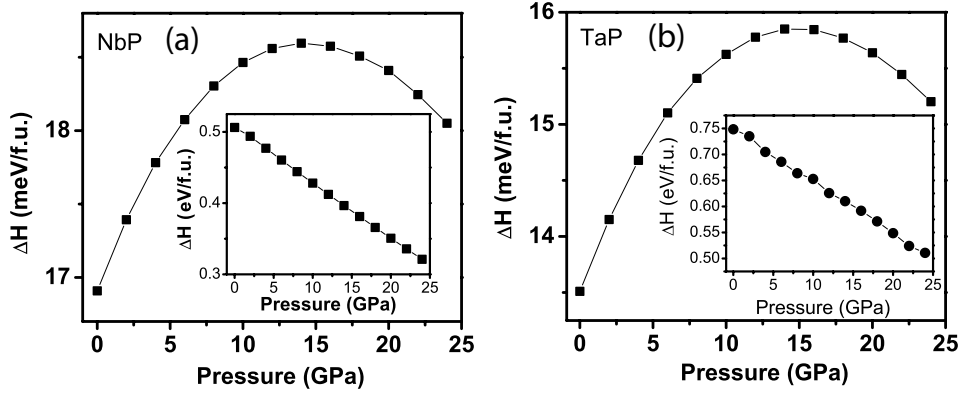


FIG. 10: (Color online) Pressure dependent difference in enthalpy of body-centered tetragonal (BCT) and hexagonal (hex) structures of NbP (a) and TaP (b). ΔH of BCT and cubic structures are given in the inset.

sition. The small changes in the electronic band topology or Fermi surface topology are driven by external parameters and reflected in the anomalies in the measurable quantities of two types: (a) the appearance or disappearance of electron and hole pockets and (b) the rupturing of necks connecting Fermi-arcs. In the present work, we observe Lifshitz transition³⁶ associated with the former.

We now present our results for pressure dependence of

Raman active modes of TaP. We show the variation of Raman active modes as a function of pressure in Fig. 6 (b). Calculated Raman active modes do not exhibit any change in S, consistent with our experimental results on TaP (Fig. 6 (a)). To further check whether TaP would undergo a structural phase transition to either the hexagonal or cubic phases, we estimated the enthalpies of BCT, cubic and hexagonal crystal structures of TaP. Although

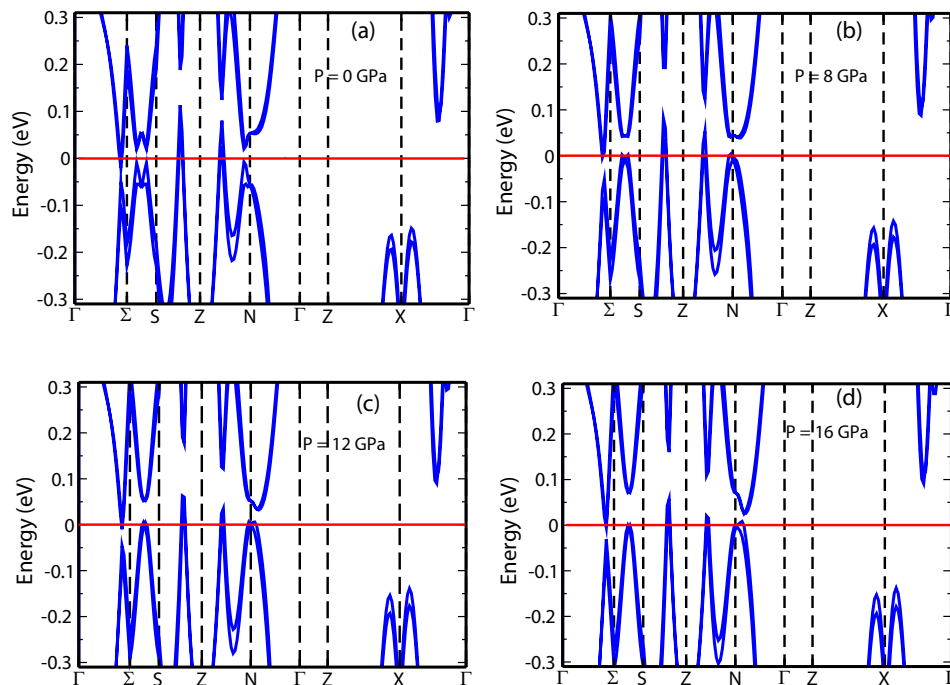


FIG. 11: (Color online) Electronic structure of bulk NbP calculated at (a) 0 GPa, (b) 8 GPa, (c) 12 GPa and (d) 16 GPa.

the enthalpy difference (ΔH) (inset of Fig. 10b) between the cubic and BCT phases decreases with pressure, it does not become negative even up to 24 GPa. Thus, a structural phase transition to the cubic phase of TaP is ruled out. Similarly, (ΔH) between the hexagonal and BCT phases (Fig. 10b) also does not exhibit a crossover to negative values, signifying absence of any structural phase transition, consistent with ours experiments.

V. SUMMARY

Frequencies of A_1 and B_1^2 modes of NbP show a change in slope ($S = \frac{d\omega}{dP}$) at P_c and its resistivity exhibits a minimum at P_c . The pressure dependent volume of NbP reveals that there is a change in the bulk modulus by ~ 36 GPa at P_c . We show that these anomalies are associated with pressure-induced Lifshitz transition at P_c

using first-principles density functional theoretical analysis. The BCT structure of NbP is robust as a function of pressure upto 24 GPa. Our experimental measurements and theoretical analysis of TaP show that its BCT structure is quite robust under pressure, and exhibits no structural or electronic phase transitions with pressure.

VI. ACKNOWLEDGMENTS

AKS thanks Department of Science and Technology, India for the financial support. AS and KP are thankful to Jawaharlal Nehru Centre for Advanced Scientific Research, India for research fellowship. UVW acknowledges support from Indo-Korea Science and Technology (IKST) Center and a J. C. Bose National Fellowship of the Department of Science and Technology, Govt of India.

* To whom correspondence should be addressed; Electronic address: asood@physics.iisc.ernet.in

¹ H. Weyl, *Zeitschrift für Physik A Hadrons and Nuclei* **56**, 330 (1929).

² H. Weng, C. Fang, Z. Fang, B. A. Bernevig, and X. Dai, *Phys. Rev. X* **5**, 011029 (2015).

³ S. Y. Xu, I. Belopolski, N. Alidoust, M. Neupane, G. Bian, C. Zhang, R. Sankar, G. Chang, Z. Yuan, C. C. Lee, S. M. Huang, H. Zheng, J. Ma, D. S. Sanchez, B. Wang, A. Bansil, F. Chou, P. P. Shibayev, H. Lin, S. Jia, and M. Z.

Hasan, *Science* **349**, 613 (2015).

⁴ B.Q. Lv, H.M. Weng, B.B. Fu, X.P. Wang, H. Miao, J. Ma, P. Richard, X.C. Huang, L.X. Zhao, G.F. Chen, Z. Fang, X. Dai, T. Qian, and H. Ding, *Phys. Rev. X* **5**, 031013 (2015).

⁵ B. Q. Lv, N. Xu, H. M. Weng, J. Z. Ma, P. Richard, X. C. Huang, L. X. Zhao, G. F. Chen, C. E. Matt, F. Bisti, V. N. Strocov, J. Mesot, Z. Fang, X. Dai, T. Qian, M. Shi and H. Ding, *Nat. Phys.* **11**, 724 (2015).

⁶ L. X. Yang, Z. K. Liu, Y. Sun, H. Peng, H. F. Yang, T.

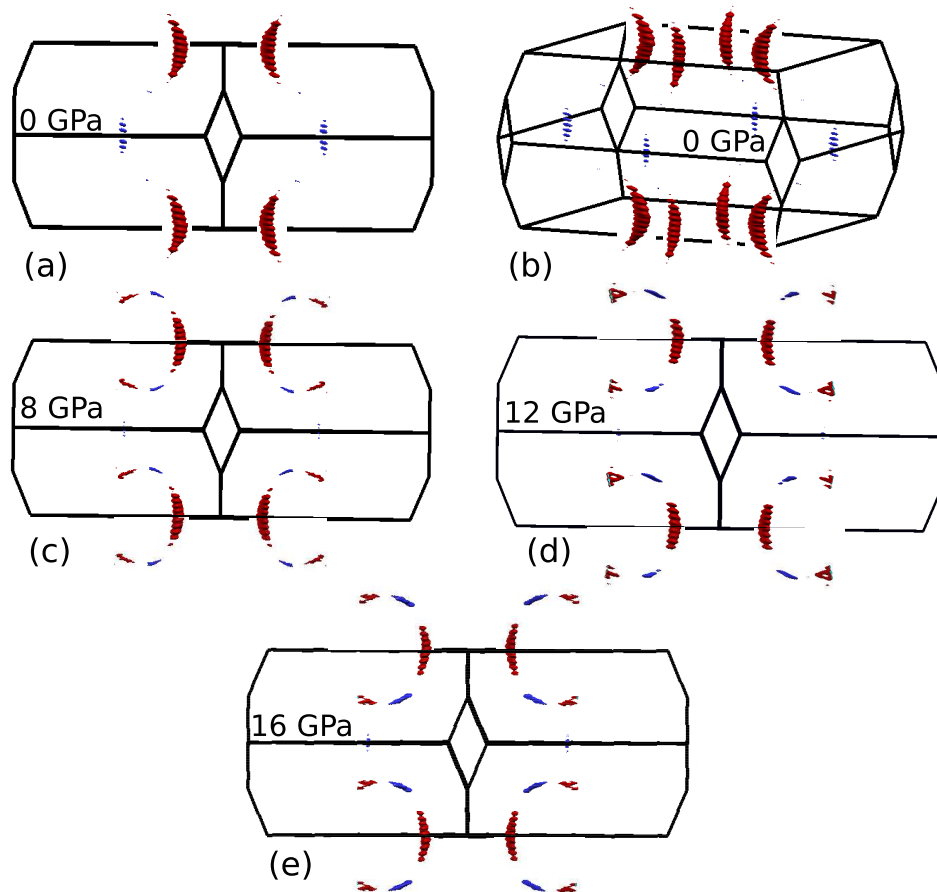


FIG. 12: (Color online) Evolution of the Fermi surface of NbP with pressure. Two views of the Fermi surface at 0 GPa (a, b). Fermi surface, at 8 GPa (c), 12 GPa (d) and 16 GPa (e) show changes in size of electron and hole pockets with pressure. Red color shows hole pockets whereas blue color shows electron pockets.

- Zhang, B. Zhou, Y. Zhang, Y. F. Guo, M. Rahn, D. Prabhakaran, Z. Hussain, S.-K. Mo, C. Felser, B. Yan and Y. L. Chen, *Nat. Phys.* **11**, 728 (2015).
- ⁷ S. Y. Xu, I. Belopolski, D. S. Sanchez, C. Zhang, G. Chang, C. Guo, G. Bian, Z. Yuan, H. Lu, T. R. Chang, P. P. Shibayev, M. L. Prokopovych, N. Alidoust, H. Zheng, C. C. Lee, S. M. Huang, R. Sankar, F. Chou, C. H. Hsu, H. T. Jeng, A. Bansil, T. Neupert, V. N. Strocov, H. Lin, S. Jia and M. Zahid Hasan, *Sci. Adv.* **1**, e1501092 (2015).
- ⁸ X. Huang, L. Zhao, Y. Long, P. Wang, D. Chen, Z. Yang, H. Liang, M. Xue, H. Weng, Z. Fang, X. Dai, and G. Chen, *Phys. Rev. X* **5**, 031023 (2015).
- ⁹ C. L. Zhang, S. Y. Xu, I. Belopolski, Z. Yuan, Z. Lin, B. Tong, G. Bian, N. Alidoust, C. C. Lee, S. M. Huang, T. R. Chang, G. Chang, C. H. Hsu, H. T. Jeng, M. Neupane, D. S. Sanchez, H. Zheng, J. Wang, H. Lin, C. Zhang, H. Z. Lu, S. Q. Shen, T. Neupert, M. Z. Hasan, and S. Jia, *Nat. Commun.* **7**, 10735 (2016).
- ¹⁰ C. Shekhar, A. K. Nayak, Y. Sun, M. Schmidt, M. Nicklas, I. Leermakers, U. Zeitler, W. Schnelle, J. Grin, C. Felser, and B. Yan, *Nat. Phys.* **8**, 645 (2015).
- ¹¹ H. B. Nielsen and M. Ninomiya, *Phys. Lett. B* **130**, 389 (1983).
- ¹² V. Aji, *Phys. Rev. B* **85**, 241101 (2012).
- ¹³ D. T. Son and B. Z. Spivak, *Phys. Rev. B* **88**, 104412 (2013).
- ¹⁴ H.-J. Kim, K.-S. Kim, J.-F. Wang, M. Sasaki, N. Satoh, A. Ohnishi, M. Kitaura, M. Yang, and L. Li, *Phys. Rev. Lett.* **111**, 246603 (2013).
- ¹⁵ P. Hosur and X. Qi, *C R Phys* **14**, 857 (2013).
- ¹⁶ S. M. Huang, S. Y. Xu, I. Belopolski, C. C. Lee, G. Chang, B. Wang, N. Alidoust, G. Bian, M. Neupane, C. Zhang, S. Jia, A. Bansil, H. Lin and M. Z. Hasan, *Nat. Commun.* **6**, 7373 (2015).
- ¹⁷ Z. Liu, L. Yang, Y. Sun, T. Zhang, H. Peng, H. Yang, C. Chen, Y. Zhang, Y. Guo, D. Prabhakaran, M. Schmidt, Z. Hussain, S.-K. Mo, C. Felser, B. Yan, and Y. L. Chen, *Nat. Mater.* **15**, 27 (2016).
- ¹⁸ S. Y. Xu, N. Alidoust, I. Belopolski, Z. Yuan, G. Bian, T. R. Chang, H. Zheng, V. N. Strocov, D. S. Sanchez, G. Chang, C. Zhang, D. Mou, Y. Wu, L. Huang, C. C. Lee, S. M. Huang, B. Wang, A. Bansil, H. T. Jeng, T. Neupert, A. Kaminski, H. Lin, S. Jia and M. Z. Hasan, *Nat. Phys.* **11**, 748 (2015).
- ¹⁹ Y. Zhou, P. Lu, Y. Du, X. Zhu, G. Zhang, R. Zhang, D. Shao, X. Chen, X. Wang, M. Tian, J. Sun, X. Wan, Z. Yang, W. Yang, Y. Zhang, and D. Xing, *Phys. Rev. Lett.* **117**, 146402 (2016).
- ²⁰ Y. Luo, N. Ghimire, E. Bauer, J. Thompson, and F. Ronning, *J. Phys. Condens. Matter* **28**, 055502 (2016).

- ²¹ R. D. dos Reis, S. C. Wu, Y. Sun, M. O. Ajeesh, C. Shekhar, M. Schmidt, C. Felser, B. Yan, and M. Nicklas, *Phys. Rev. B* **93**, 205102 (2016).
- ²² J. Martin and R. Zum Gruehn, *Z. Kristallogr* **182**, 180 (1988).
- ²³ F. Arnold, C. Shekhar, S. C. Wu, Y. Sun, R. D. d. Reis, N. Kumar, M. Naumann, M. O. Ajeesh, M. Schmidt, A. G. Grushin, J. H. Bardarson, M. Baenitz, D. Sokolov, H. Borrmann, M. Nicklas, C. Felser, E. Hassinger and B. Yan, *Nat. Commun.* **7**, 11615 (2016).
- ²⁴ P. Giannozzi *et al.*, *J. Phys. Condens. Matter* **21**, 395502 (2009).
- ²⁵ D. Vanderbilt, *Phys. Rev. B* **41**, 7892 (1990).
- ²⁶ J. P. Perdew and A. Zunger, *Phys. Rev. B* **23**, 5048 (1981).
- ²⁷ A. DalCorso and A. MoscaConte, *Phys. Rev. B* **71**, 115106 (2005).
- ²⁸ H. Boller and E. Parth, *Acta Crystallogr.* **16**, 1095 (1963).
- ²⁹ H. Liu, P. Richard, L. Zhao, G. Chen, and H. Ding, *J. Phys. Condens. Matter* **28**, 295401 (2016).
- ³⁰ V. Petricek, M. Dusek, and L. Palatinus, *Z. Kristallogr.* **229**(5), 345 (2014).
- ³¹ W. Xiaoa, D. Tana, X. Xionga, J. Liub and J. Xuc, *Proc. Natl. Acad. Sci.* **107**, 14026 (2010)
- ³² J. Zhao, L. Xu, Y. Liu, Z. Yu, C. Li, Y. Wang, and Z. Liu, *J. Phys. Chem. C* , **119**, 27657 (2015).
- ³³ F. Hong, B. Yue, N. Hirao, G. Ren, B. Chen and H. K. Mao, *Appl. Phys. Lett.* **109**, 241904 (2016).
- ³⁴ C. C. Lee, S. Y. Xu, S. M. Huang, D. S. Sanchez, I. Belopolski, G. Chang, G. Bian, N. Alidoust, H. Zheng, M. Neupane, B. Wang, A. Bansil, M. Z. Hasan, and H. Lin, *Phys. Rev. B* **92**, 235104 (2015).
- ³⁵ A. Bera, A. Singh, D. V. S. Muthu, U. V. Waghmare and A. K. Sood, *J. Phys. Condens. Matter* **29**, 105403 (2017).
- ³⁶ I. M. Lifshitz, *Sov. Phys. JETP* **11**, 1130 (1960).